Stochastic Environmental Research and Risk Assessment (2026) 40:147
https://doi.org/10.1007/s00477-026-03280-5

ORIGINAL PAPER

Scale-dependent phase reversal in climate–CO_2 relationships: evidence from long-term spectral analysis of urban climate data

Isabella Morlini[1] · **Stefano Orlandini**[2]

Received: 10 January 2026 / Accepted: 14 May 2026

Abstract

Understanding the stochastic variability of climate–carbon relationships across temporal scales remains a key challenge in climate analysis. This study investigates scale-dependent interactions between local temperature, precipitation, and atmospheric CO_2 concentrations using long-term observations from Modena (Italy) and regional and global datasets. Cross-spectral analysis reveals dominant 12-month periodicities in local temperature associated with regional CO_2 variability, as well as 3.5- and 4–5-year periodicities linked to global CO_2 fluctuations. A consistent scale-dependent phase reversal emerges across temporal scales, with CO_2 leading temperature at annual and sub-18-month periods and temperature often leading CO_2 at interannual timescales. This behavior provides a coherent framework for distinguishing relationships driven by shared seasonal forcing from those emerging through longer-term feedback mechanisms. In contrast, associations between CO_2 (both local and global) and precipitation dynamics remain limited and intermittent, with largely decoupled periodicities across scales. The analysis also reveals changes in the intra-annual variability of temperature range and precipitation after 2001, indicating a reorganization of local climate dynamics. Overall, the results show that climate–carbon relationships are strongly scale-dependent and highlight the value of frequency-domain approaches for characterizing variability and avoiding misleading inferences in non-stationary, multi-scale environmental time series.

1 Introduction

Rainfall and temperature are the two primary climatic variables affected by climate change, with impacts that vary across local contexts (Bharghavi et al. 2025; Esit et al. 2025; Hua et al. 2008; Kalnay & Cai 2003; Katavoutas et al. 2023). Understanding the variability, trends, and long-term changes in precipitation and temperature is essential for accurate hydrological modeling under changing climate conditions (Mumo et al. 2019), and temporal analyses of meteorological data are crucial for detecting persistent climatic shifts (Shrestha et al. 2019). As outlined by Speer and Leslie (2024), the spatial heterogeneity of global warming necessitates a reassessment of climate periods, an investigation of emerging patterns of temperature and precipitation unseasonality, and a revision of climate definitions at the local scale. In the context of sustainable development, particularly in urbanized areas, it is also important to assess the influence of regional external forcings such as greenhouse gas emissions resulting from human activities. Atmospheric carbon dioxide (CO_2) is considered the most significant greenhouse gas in terms of warming potential and anthropogenic contribution (Gogeri et al. 2024). However, understanding the temporal dynamics of CO_2 and their effects on local temperature and precipitation remains challenging, as these influences are complex and vary across timescales. Moreover, as noted by Varotsos et al. (2007), fluctuations in CO_2 concentrations exhibit long-range power-law correlations (long memory), which may lead to spurious relationships. In recent years, spectral analysis (Priestley 1981; Thomson 1982; Percival & Walden 1993) has been increasingly applied to improve the characterization of the dynamics and variability of climatic time series (Wu et al. 1995; Mann & Lee, 1996; Olafsdottir et al. 2016; Lopes et al., 2018), as well as CO_2 concentrations (Kivi et al., 2016; Pili & Violanda 2020; Zhang et al. 2021). However, relationships inferred in the time domain may conceal

✉ Isabella Morlini
isabella.morlini@unimore.it

[1] Dipartimento Di Comunicazione Ed Economia, Università Degli Studi Di Modena E Reggio Emilia, Reggio Emilia, Italy

[2] Dipartimento Di Ingegneria Enzo Ferrari, Università Degli Studi Di Modena E Reggio Emilia, Modena, Italy

Published online: 03 June 2026

fundamentally different behaviors across temporal scales, including potential reversals in phase relationships that can lead to misleading interpretations.

When examining relationships between climatic time series, accurate estimation of time shifts is essential for understanding temporal dependencies and potential causal links. Cross-power spectral analysis provides a robust framework for identifying correlations in the frequency domain and quantifying phase differences between two series. The phase difference at a given frequency indicates their temporal alignment: zero denotes synchronicity, whereas positive or negative values indicate leading or lagging behavior. In this study, we employ cross-spectral analysis to investigate interactions between local and global climate variables, with particular focus on intra and interannual variability and the role of atmospheric CO_2. To achieve this, we adopt a frequency-domain approach, which allows separation of long-term trends from cyclical components and reduces the risk of confounding effects due to non-stationary noise. Local climatic variables are derived from observations collected in the city of Modena, Italy, which provides a representative case study of urban heat island dynamics (Morlini et al. 2024; Costanzini et al. 2024). This study extends the results previously reported by Morlini et al. (2023, 2025) on air temperature and precipitation in Modena by further examining the interactions between these local climatic variables and both local and global CO_2 concentrations. Notably, local CO_2 measurements used in this study, obtained from the Monte Cimone station (2165 m a.s.l.), represent regional background concentrations rather than urban-scale CO_2 variability in Modena. In this work, CO_2 is not intended to represent local urban emissions but rather a large-scale atmospheric signal that provides a consistent reference for investigating scale-dependent relationships with locally observed temperature and precipitation. This approach is consistent with established literature characterizing the differences between urban, rural, and regional background CO_2 records in mid-latitude environments (Velasco and Roth 2010; Arizpe et al. 2021), ensuring that the observed interactions reflect broader atmospheric forcings rather than site-specific anthropogenic noise.

The main objectives of this study are as follows: (a) to analyze long-term patterns in temperature, precipitation, and CO_2 in order to appropriately preprocess the data prior to applying spectral methods; (b) to investigate changes in seasonality and modes of variability of temperature (minimum, maximum, mean, and range), precipitation depth, and local CO_2 over the past two decades; (c) to examine statistical relationships between CO_2 and temperature, and between CO_2 and precipitation depth, with the aim of identifying potential causal links; (d) to assess the scale-dependent variability of local temperature and precipitation, together with global temperature, over the period 1979–2024. Particular attention is given to dominant periodicities and their association with interannual climate drivers, including local and global CO_2; (e) to provide insights into the complex interactions between local climatic variables and global CO_2 and temperature, with specific emphasis on distinguishing the effects of global versus local CO_2 on local temperature.

While the methodological tools employed in this study are well established, the contribution of this work lies in the systematic identification of scale-dependent phase reversal and its consistent interpretation across local and global climate–carbon interactions. In particular, the analysis shows how these tools can be combined to distinguish between relationships driven by shared seasonal forcing and those emerging at interannual scales, thereby reducing the risk of misleading inference based on time-domain analysis alone. This perspective provides a coherent framework for interpreting cross-scale climate variability and highlights a non-trivial analytical outcome that is not typically emphasized in similar studies. Although the analysis is based on a case study (Modena), the methodological approach and resulting insights are intended to be transferable to other urban and mid-latitude environments characterized by similar interactions between local climate variability and large-scale atmospheric signals. The exceptionally long-term dataset further enables the identification of previously unreported features in the behavior of climatic variables over the past 46 years. By adopting a classical spectral framework, the study ensures methodological consistency and direct comparability with existing climatological literature, including foundational work on CO_2–temperature coherence (Kuo et al. 1990) and broader analyses linking local European climate records to global atmospheric forcings (Stips et al. 2016), while avoiding the interpretative complexities often associated with more recent time–frequency approaches (Jevrejeva et al. 2003).

Data and methods are described in Sect. 2, results are presented in Sect. 3, the discussion is provided in Sect. 4, and conclusions are drawn in Sect. 5.

2 Data and methods

2.1 Data

Continuous daily observations of local air temperature (*LT*) and cumulative precipitation (*P*) have been recorded at the Geophysical Observatory of the University of Modena and Reggio Emilia (44.6474° N, 10.9293° E; 76.5 m a.s.l.), Modena, Italy, since 1861 and 1830, respectively. From these records, monthly and annual time series were derived. In this study, the analysis focuses on the period

from 1979 onward to ensure consistency with the availability of the other climatic variables considered. Minimum and maximum temperatures, as well as temperature range, are analyzed at the monthly scale, while mean temperature and precipitation depth are examined at both monthly and annual resolutions. Annual and monthly time series of local atmospheric CO_2 concentrations (*LC*) were obtained from the Monte Cimone Observatory, a strategic site of the Italian Air Force Meteorological Service located at 2165 m a.s.l. on the highest peak of the Northern Apennines (44° 11′ 03″ N, 10° 42′ 00″ E; WGS84). Operational since 1937, the observatory plays a key role in meteorological forecasting, climatological monitoring, and atmospheric composition research. Monte Cimone is a reference station for background greenhouse gas measurements (Cristofanelli et al. 2013; 2021; 2024) and contributes to the World Meteorological Organization's Global Atmosphere Watch (GAW) Programme (World Meteorological Organization/Global Atmosphere Watch 2003). It is also part of the Italian Meteorological Network operated by the Air Force Meteorological Service (SYNOP 16134; METAR LIVC). Limited missing *LC* data for 2007, 2010, and 2013, occurring over very short intervals, were estimated using a moving-average interpolation. To evaluate the sensitivity of spectral estimates to gap-filling choices, alternative treatments were also considered, including linear interpolation and cubic spline interpolation. These comparisons allowed assessment of the robustness of the inferred spectral and cross-spectral features. CO_2 data obtained from the Monte Cimone station is representative of regional background atmospheric concentrations. These data are therefore interpreted as a large-scale forcing signal, while temperature and precipitation are analyzed at the local (urban) scale.

Global atmospheric CO_2 concentrations (*GC*) were obtained from measurements at the Mauna Loa Observatory, Hawaii (19.5362° N, 155.5763° W; 3397 m asl), providing the reference global CO_2 time series. Global surface temperature anomalies from 1979 onward were taken from the NASA GISS Surface Temperature Analysis (GISTEMP) dataset. To enable direct comparison with local observations, a reconstructed global temperature series for Modena (*GT*) was obtained by adding the mean local temperature observed during the 1951–1979 baseline period ($T_b = 13.38$ °C) to the GISTEMP anomalies. This approach, previously adopted by Morlini and Orlandini (2025), allows consistent comparison between global-scale temperature variability and local temperature observations in Modena. The dataset includes 549 monthly observations spanning March 1979 to November 2024, and 46 annual observations covering the period from 1979 to 2024. It should be noted that the reconstructed global temperature series (GT), obtained by combining global anomalies with a local baseline, is introduced solely to enable direct comparison with local observations. This transformation does not imply that the resulting series represents location-specific global conditions, and it does not account for spatial heterogeneity in global temperature patterns. Accordingly, GT should be interpreted as a large-scale reference signal rather than a locally representative variable.

2.2 Methods

To investigate periodic behavior and relationships among climatic variables, spectral analysis was applied to the time series of temperature, CO2 concentration, and precipitation. Spectral analysis decomposes a time series $\{X_t\}$ (t = 1, …, *N*) into a sum of sinusoidal components with uncorrelated random coefficients, allowing the identification of dominant cycles and oscillatory patterns that may not be evident in the time domain. This representation also expresses the autocovariance and autocorrelation functions as sums of sinusoidal components. Because the spectral density is formally defined for continuous-time processes, while the available observations consist of a finite number of equally spaced measurements, the analysis is based on the discrete Fourier transform (DFT). The DFT provides an empirical approximation of the underlying spectral properties of the time series. The Fourier cosine and sine coefficients at each Fourier frequency ω_k are computed as follows:

$$\omega_k = \frac{2\pi k}{N}, k = -\frac{N-1}{2}, \cdots, \frac{N}{2}$$

$$a_k = \frac{2}{N}\sum_{t=1}^{N} X_t \cos\left(\omega_k\left(t-1\right)\right)$$

$$b_k = \frac{2}{N}\sum_{t=1}^{N} X_t \sin\left(\omega_k\left(t-1\right)\right)$$

The periodogram I_k, which represents the raw spectral estimate, is then computed as:

$$I_k = \frac{N}{2}\sum_{t=1}^{N}(a_k^2 + b_k^2)$$

A smoothed spectral density estimate $\widehat{f_k}$, also referred to as a discrete spectral average, is obtained from the periodogram through a weighted averaging procedure:

$$\widehat{f_k} = \sum_{i=-p}^{p}\left(w_i J_{k+1}\right), J_{k+1} = \begin{cases} I_{k+i} & 0 \le k+i \le N \\ I_{-(k+i)}, & k+1 < 0 \\ I_{N-(k+i)}, & k+1 > 0 \end{cases}$$

Here, p denotes the bandwidth, and w_i are weights determined by the choice of smoothing kernel. Commonly used kernels include the following. Bartlett kernel is given by:

$$\begin{cases} c = 1/2 & e = 1/3 \\ w_i = 1 - |\lambda_i| & if|\lambda_i| \le 1 \\ w_i = 0 & otherwise \end{cases}$$

Parzen kernel is given by:

$$\begin{cases} c = 1 & e = 1/3 \\ w_i = 1 - 6|\lambda_i|^2 + 6|\lambda_i|^3 & if|\lambda_i| \le 0.5 \\ w_i = 2(1 - |\lambda_i|)^3 & if 0.5 \le |\lambda_i| \le 1 \\ w_i = 0 \quad otherwise \end{cases}$$

Quadratic spectral is given by:

$$\begin{cases} c = 1/2, e = 1/5 \\ w_i = \frac{25}{12\pi^2\lambda_i^2}\left(\frac{\sin\left(\frac{6\pi\lambda_i}{5}\right)}{\left(\frac{6\pi\lambda_i}{5}\right)} - \cos\left(\frac{6\pi\lambda_i}{5}\right)\right) \end{cases}$$

Tukey-Hanning is given by:

$$\begin{cases} c = 2/3 & e = 1/5 \\ w_i = (1 + \cos(\pi\lambda_i))/2 & if|\lambda_i| \le 1 \\ w_i = 0 & otherwise \end{cases}$$

Truncated kernel is given by:

$$\begin{cases} c = 1/4 & e = 1/5 \\ w_i = 1 & if|\lambda_i| \le 1 \\ w_i = 0 & otherwise \end{cases}$$

The bandwidth p is defined as $p = c \cdot q$, where $q = N/2 + 1$, and $\lambda_i = i/p$ ($i = 1,\ldots,q$). The weights w_i are positive and sum to one, ensuring that the resulting spectral estimate provides a consistent and unbiased representation of the underlying frequency structure of the time series. Fourier cosine and sine transform, together with the derived spectral functions, were computed using XLSTAT (Addinsoft 2023). If a second time series $\{Y_t\}$ is available, several additional functions can be computed to estimate the cross-spectrum. The real part of the cross-periodogram of the time series X_t and Y_t is given by $\text{Real}_k = \sum_{t=1}^{n}(a_t a_t' + b_t b_t')$, while the imaginary part is given by $\text{Imag}_k = \sum_{t=1}^{n}(a_t b_t' - b_t a_t')$. The cospectrum estimate (i.e., the real part of the cross-spectrum) of X_t and Y_t is given by:

$$C_k = \sum_{i=-p}^{p} w_i R_{k+i}$$

where the following notation applies:

$$R_{k+i} = \begin{cases} Real_{k+i}, & 0 \le k+i \le n \\ Real_{k+i}, & k+i < 0 \\ Real_{k+i}, & k+i > n \end{cases}$$

Similarly, the quadrature spectrum estimate (i.e., the imaginary part of the cross-spectrum) is given by:

$$Q_k = \sum_{i=-p}^{p} w_i H_{k+i}$$

with the weights w_i defined as:

$$w_i = \begin{cases} \frac{1+\cos(\pi\lambda_i)}{2} & |\ \lambda_i\ | \le 1 \\ 0 & \text{otherwise} \end{cases}$$

or alternatively:

$$w_i = \begin{cases} 1 & |\ \lambda_i\ | \le 1 \\ 0 & \text{otherwise} \end{cases}$$

The phase of the cross-spectrum between X_t and Y_t is given by:

$$\phi(\lambda) = \arctan\frac{Q(\lambda)}{C(\lambda)}$$

The amplitude of the cross-spectrum is given by:

$$|\ S_{XY}(\lambda)\ | = \sqrt{C^2(\lambda) + Q^2(\lambda)}$$

The squared coherence between the two-time series is given by:

$$\gamma^2(\lambda) = \frac{|\ S_{XY}(\lambda)|^2}{S_{XX}(\lambda)S_{YY}(\lambda)}$$

A negative phase indicates that variations in X_t lead changes in Y_t, whereas a positive phase indicates the opposite.

Although the theoretical significance of squared coherence can be evaluated using the Beta distribution (Jenkins & Watts 1968), caution is warranted in climate applications because of the strong autocorrelation typically present in climatic time series and the large degrees of freedom introduced by spectral smoothing. In this study, quadratic spectral smoothing was applied to 548 observations (the number of monthly first differences) using parameters $c = 0.5$ and $e = 0.2$, together with the following discretization:

$$p = c \bullet q, q = \frac{548}{2} + 1, \lambda_i = \frac{i}{p}, i = 1, \cdots q$$

The bandwidth is computed as (Bloomfield 2000; Sargent 1987) $b = c \times 548^{-e} = 0.5 \times 548^{-0.2} \approx 0.1416$, indicating that the smoothing spans approximately 14% of the Nyquist frequency. The effective degrees of freedom for the Beta distribution are estimated as: $\nu = 2 \times (0.1416 \times 548) = 155.2$. The corresponding critical values for the squared coherence (Bendat & Piersol 2011) are C^2_{crit} = 0.038 at 5% significance level, and 0.057 at 1%. Considering 45 observations (first differences of annual values) and quadratic spectral smoothing (with parameters $c = 0.5$ and $e = 0.2$), the resulting bandwidth $(b = c \cdot 45^{-e} = 0.5 \times 45^{-0.2} \approx 0.2335)$ indicates that the smoothing spans approximately 23% of the Nyquist frequency. The effective degrees of freedom for the associated Beta distribution were then estimated $(\nu = 2\,(b \cdot 45) \approx 21.0)$, and the corresponding critical values for the squared coherence were determined. At the 5% significance level, the threshold is $\gamma^2_{crit} = 0.27$, and at 1% it is 0.39. With such extensive smoothing and a high number of degrees of freedom, the significance thresholds become very low. As a result, even relatively small coherence values may appear statistically significant (values as small as 0.1 are statistically significant at the 5% level). A large number of degrees of freedom indicates that the smoothing procedure produces stable coherence estimates but reduces sensitivity to short-term oscillations. From a practical standpoint, coherence values exceeding 0.1 can therefore be regarded as statistically significant. When degrees of freedom based on segment averaging without smoothing are applied (equal to 2 K, where K is the number of independent segments), the critical coherence values vary substantially. At α=0.05, they range from 0.78 (182.7-month period) to 0.07 (11.9-month period). At α=0.01, they range from 0.9 to 0.1. For annual series, the critical coherence values range from 0.31 (for the 5-year period) to 0.14 (for the 2-year period) at α=0.05, and from 0.44 to 0.20 at α=0.01. These results support the view that strict statistical tests of coherence may not be fully appropriate for climatic time series. Accordingly, in this study, coherence values are reported primarily for descriptive purposes, while their robustness is assessed based on consistency across neighboring frequency bands and their physical interpretability. For this reason, formal significance thresholds are not used as the primary basis for interpretation. Instead, coherence is evaluated based on consistency across adjacent frequency bands and physical interpretability. In particular, we prioritize the interpretation of coherence peaks exceeding 0.6, ensuring that the identified relationships reflect robust physical couplings (e.g., NAO-related variability and CO_2 forcings) rather than marginal statistical artifacts.

To identify both short-term oscillations (e.g., seasonal cycles) and long-term patterns (e.g., multi-year or decadal variability), as well as to evaluate temporal relationships and potential causality among climatic variables, the time series must be detrended and approximately white noise. During the preprocessing stage, several tests were applied to detect the presence of trends, after which the series were detrended using first-order differencing. In addition, Fisher's Kappa test (Fisher 1929; Fuller 1976) and Bartlett's Kolmogorov–Smirnov test (Bartlett, 1967) were used to assess whether the detrended series could be reasonably approximated as white noise. The tests provided evidence against the white noise hypothesis, indicating that the detrended series retain non-random variability and can be considered suitable for spectral analysis. To assess homoscedasticity, a linear regression on time was fitted to the transformed data. The Breusch–Pagan and White tests were then applied to the residuals (Breusch and Pagan 1979; White 1980; Greene, 2018; Douglas et al. 2021). In all cases, the tests yielded *p*-values greater than 0.1, indicating no statistically significant evidence of heteroscedasticity. Therefore, also the assumption of constant variance can be considered reasonable for the subsequent spectral analysis.

To assess the robustness of the spectral results, the analysis was conducted using two alternative detrending approaches. In addition to the spectra computed from the first-differenced series, spectral analysis was also applied to the residuals obtained after removing the trend component estimated through a linear Holt–Winters model (Holt 2004; Winters 1960; Hyndman and Athanasopoulos 2018), with the smoothing parameters (α and β) estimated using the Levenberg–Marquardt non-linear optimization algorithm (Nocedal and Wright 2006). The procedure was repeated using residuals derived from centered moving-average filtering. To ensure consistency across datasets with different temporal resolutions, the window length was adjusted to represent the same physical timescale. Specifically, a 36-month window was used for monthly data, corresponding to a 3-year window for annual data. All resulting series were subsequently tested against the white noise hypothesis using Fisher's Kappa and Bartlett's Kolmogorov–Smirnov tests and were further examined for the presence of residual trends and heteroscedasticity. The comparison among these different preprocessing methods allowed evaluation of the stability of the detected periodicities and coherences with respect to the choice of detrending technique.

Seasonality removal was intentionally not applied in this study. For the annual data, seasonal effects are inherently absent due to temporal aggregation. For the monthly series, the analysis was explicitly designed to investigate potential changes in seasonal variability by comparing the most recent 23-year period with the preceding 23-year interval. Therefore, preserving the seasonal component was methodologically necessary to ensure that any differences in

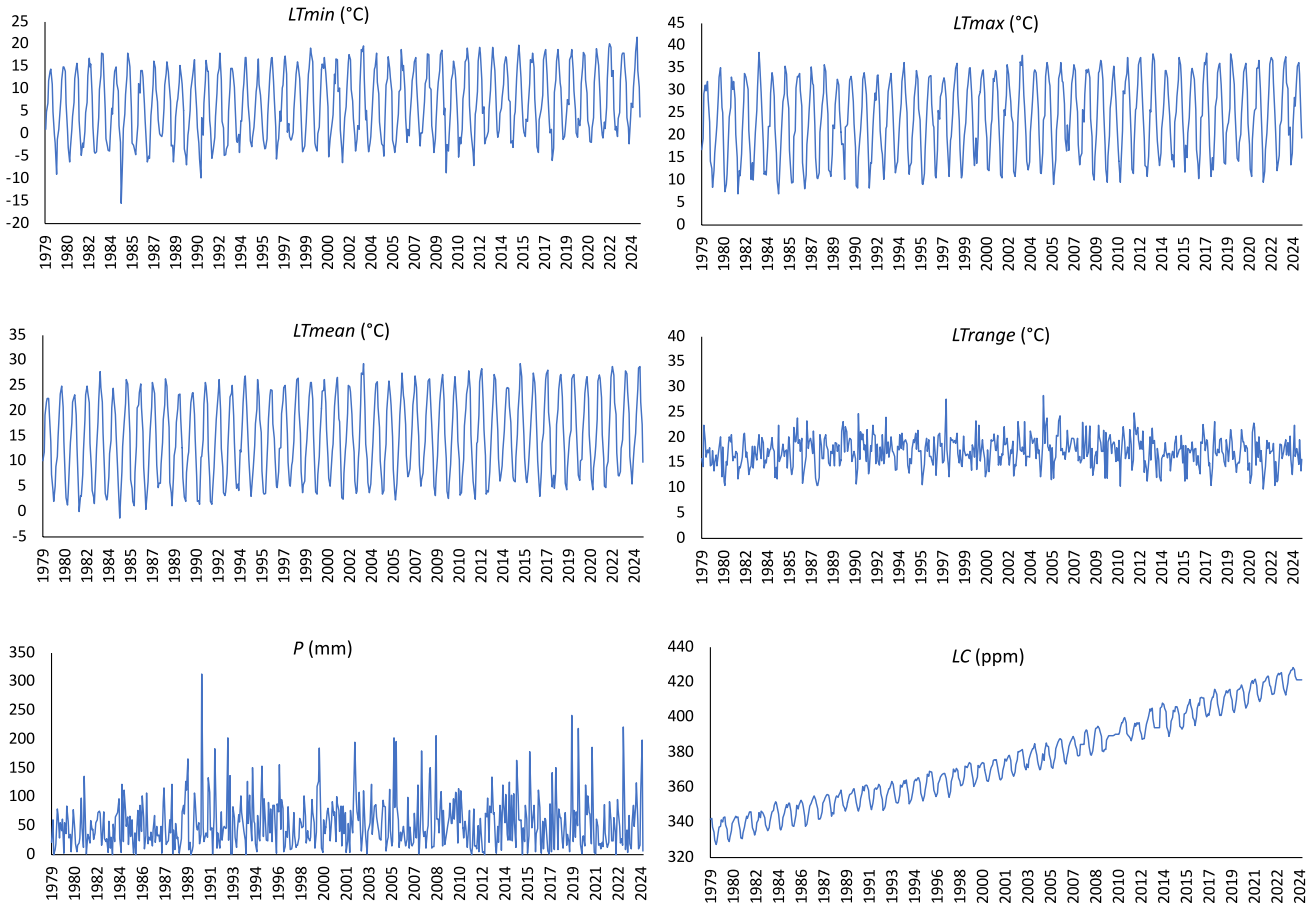

Fig. 1 Monthly time series of local minimum temperature (*LTmin*), maximum temperature (*LTmax*), mean temperature (*LTmean*), temperature range (*LTrange*), precipitation depth (*P*), and local CO_2 concentration (*LC*)

spectral characteristics between the two periods could be attributed to genuine changes in seasonality rather than to preprocessing choices.

Specifically, we opted for Fourier analysis to circumvent the constraints of dyadic scale partitioning inherent in discrete wavelet transforms (e.g., MODWT). While wavelets are effective for non-stationary signals, they aggregate spectral information into fixed octave bands (such as 8–16 or 32–64 months), which can blur the identification of exact periodicities. In contrast, the finer and continuous frequency resolution of the Fourier transform allows us to precisely isolate specific oscillations, such as the annual cycle and multi-year fluctuations, without the artifacts potentially introduced by dyadic partitioning.

3 Results

3.1 Monthly series

Monthly time series of local minimum temperature (*LTmin*), maximum temperature (*LTmax*), mean temperature (*LTmean*), temperature range (*LTrange*), precipitation depth (*P*), and local CO_2 concentration (*LC*) are shown in Fig. 1. The statistical assessment of the presence or absence of monotonic trends, inhomogeneities, and change points was conducted using several nonparametric tests implemented in XLSTAT (Addinsoft 2023). Summary results of the Mann–Kendall (MK) test (Mann 1945; Kendall, 1975; Gilbert 1987) and the von Neumann test (von Neumann 1941) are reported in Table 1. Neither the MK test nor the von Neumann test requires the data to be normally distributed, nor do they assume linearity of the trend, if present.

Table 1 Summary results of the Mann–Kendall and von Neumann trend tests

Series	Mann–Kendall trend test		von Neuman test
	p-value	Sen's slope	*p*-value
LTmin (°C)	**<0.0001**	0.007	**<0.0001**
LTmax (°C)	**<0.0001**	0.008	**<0.0001**
LTmean (°C)	**<0.0001**	0.007	**<0.0001**
LTrange (°C)	0.815	0.000	**<0.0001**
P (mm)	0.367	0.008	0.020
LC (ppm)	**<0.0001**	0.160	**<0.0001**

The null hypothesis for both tests is that the data consist of independent and identically distributed observations. The alternative hypothesis for the MK test is the presence of a monotonic trend, whereas for the von Neumann test it is that the observations are not randomly distributed and exhibit serial correlation. For the von Neumann test, *p*-values were estimated using 10,000 Monte Carlo simulations. The Sen's slope estimator (Sen 1968; Hipel & McLeod 1994) was used to quantify the linear rate of change associated with the MK test. Results indicate that the *LTmin*, *LTmax*, and *LTmean* series exhibit statistically significant deterministic linear trends, with *LTmin* and *LTmean* increasing by approximately 0.007 °C per month and *LTmax* increasing, on average, by 0.008 °C per month. Both tests indicate departures from first-order stationarity in the CO_2 (*LC*) series, which shows an average increase of 0.160 ppm per month. In contrast, no statistically significant trend was detected for precipitation depth (*P*) at the 1% significance level. This finding is consistent with the lack of a clear trend in total precipitation observed across Italy, as reported by Caporali et al. (2021). For the temperature range (*LTrange*) series, the results are not fully consistent: while the Mann–Kendall test does not detect a significant trend, the von Neumann test indicates the presence of non-stationarity.

Summary results of the Pettitt (Pettitt 1979; Verstraeten et al. 2006), Buishand (Buishand 1982, 1984), and SNHT (Standard Normal Homogeneity Test; Haimberger 2007) tests for detecting shifts in central tendency are reported in Table 2. For all three tests, the null hypothesis assumes that the observations follow one or more distributions sharing the same location parameter μ (i.e., no change point). The alternative hypothesis assumes the existence of a change point *t*, such that the time series is characterized by a location parameter μ_1 before *t* and a different location parameter μ_2 after *t*. *P*-values were estimated using 10,000 Monte Carlo simulations.

These three tests further support the hypothesis of nonstationarity in the *LTmin*, *LTmax*, *LTmean*, and *LC* series, and first-order stationarity in the *P* and *LTrange* series. Although the change points identified by the tests differ slightly, they consistently reject the null hypothesis of a constant location parameter over time for all series except *P* and *LTrange*. For *LTmin*, the change points identified by the three tests are identical or differ by only one month. For *LTmax*, *LTmean*, and *LC*, the change points differ by at most one year. The earliest change point detected in the CO_2 series occurs in 2001. Notably, this breakpoint not only represents the first statistically significant shift in the record but also divides the series into two segments of approximately equal length before and after this year. To investigate potential changes in intra-annual variability beyond shifts in the mean level, spectral density estimates were compared between the subperiods 1979–2001 and 2002–2024. Spectral analysis was applied to first-differenced series to prevent the trend component from overwhelming the cyclic component.

All previously applied tests consistently reject the presence of a trend in the first-difference series; for brevity, detailed results are not reported here. The Fisher's Kappa and Bartlett's Kolmogorov–Smirnov tests indicate that the white noise hypothesis can be rejected and all subseries can be reasonably regarded as retaining non-random variability. To assess the assumption of homoscedasticity, a linear regression on time was subsequently fitted to the transformed data, and the Breusch–Pagan and White tests were applied to the residuals of the regression model. In all cases, the tests yielded *p*-values much greater than 0.1, with the sole exception of precipitation depth (with a *p*-value greater than 0.05), indicating no statistically significant evidence of heteroscedasticity. Therefore, the assumption of constant variance can be considered reasonable for the subsequent spectral analysis.

Figure 2 shows the spectral density estimates for periods ranging from 2 to 14 months, highlighting intra-annual variability. The reported spectra were estimated using the quadratic spectral kernel. Comparable spectral shapes were obtained using the Truncated, Parzen, Bartlett, and Tukey–Hanning kernels (Andrews 1991). A comparison of the spectral density pairs reveals that *LTmin*, *LTmax*, and *LTmean* exhibit a stable intra-annual structure, characterized by a single dominant peak at the 12-month period. The amplitude of this annual peak remains nearly unchanged between the two subperiods (1979–2001 and 2002–2024), indicating a persistent seasonal temperature cycle. In contrast, marked differences emerge for *LTrange*, *P*, and *LC*. In the *LC* series, the spectral peak at the 6-month period becomes negligible in the 2002–2024 interval, while the

Table 2 Summary results of the Pettitt's and Buishand's tests

	Pettitt's test		Buishand's test		SNHT test	
Series	*p*-value	*t*	*p*-value	*t*	*p*-value	*t*
LTmin (°C)	**0.015**	March 1999	**0.007**	April 1999	**0.031**	April 1999
LTmax (°C)	**0.018**	February 1997	**0.008**	February 1997	**0.031**	March 1996
LTmean (°C)	**0.038**	April 1997	**0.020**	April 1997	**0.067**	April 1996
LTrange (°C)	0.291	January 1986	0.142	February 1988	0.119	January 1986
P (mm)	0.300	March 1989	0.053	March 1989	0.101	March 1989
LC (ppm)	**<0.0001**	October 2001	**<0.0001**	October 2002	**<0.0001**	October 2002

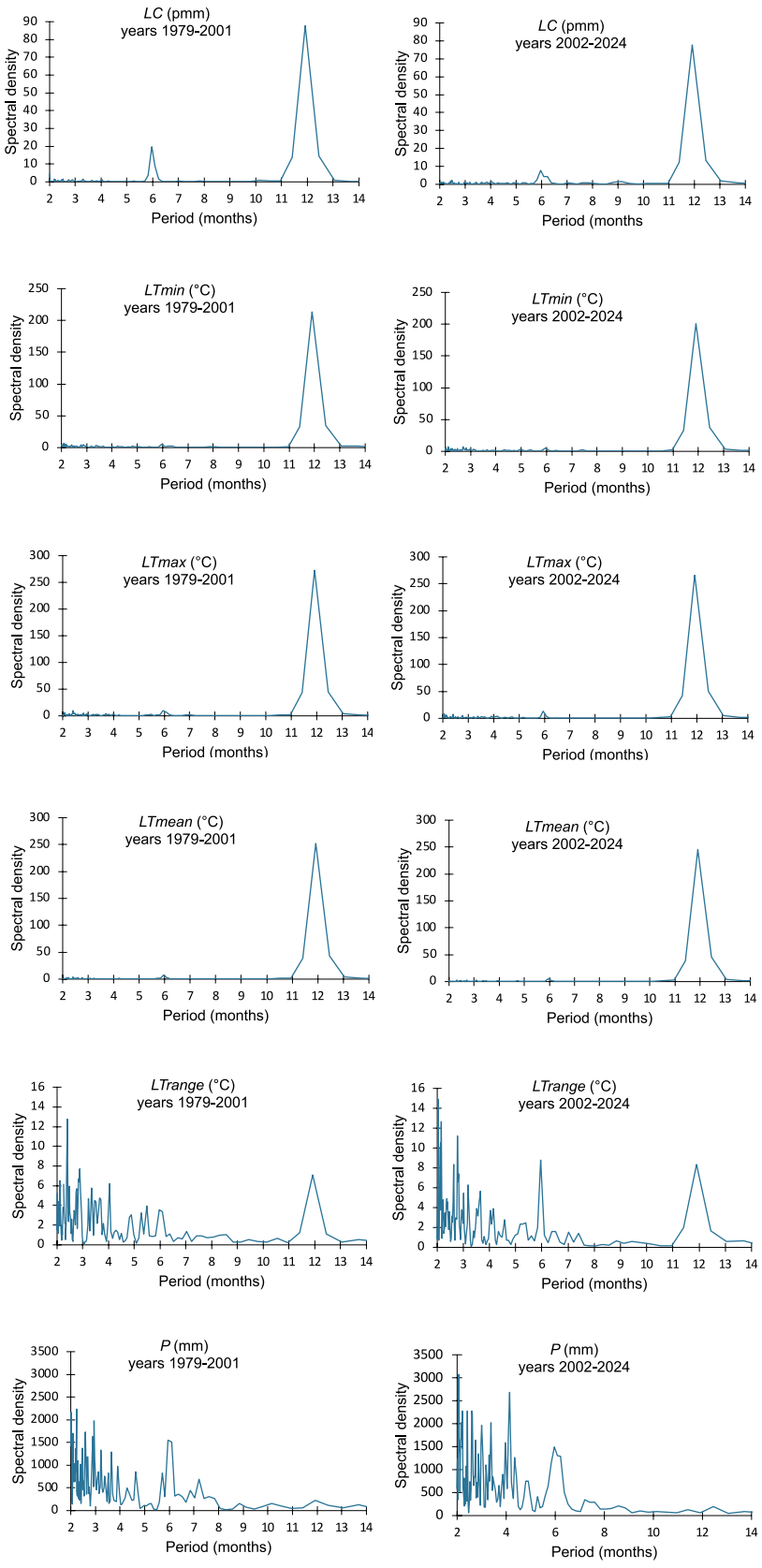

Fig. 2 Spectral densities of local CO_2 (*LC*), local minimum temperature (*LTmin*), local maximum temperature (*LTmax*), local mean temperature (*LTmean*), local temperature range (*LTrange*), and local precipitation depth (*P*) for the periods 1979–2001 and 2002–2024

annual (12-month) peak is noticeably attenuated during the same period. The temperature range (*LTrange*) displays particularly pronounced changes in seasonal variability, which may represent a meaningful indicator of ongoing climate change. Specifically, during 1979–2001, the dominant cyclic components occur at periods between 2 and 3 months, as well as at 4 and 12 months. In the more recent period (2002–2024), four prominent components emerge at 2, 2.8, 6, and 12 months, indicating a more complex seasonal structure. A similar transformation is observed in the precipitation series: over the last 22 years, new cyclic components at 2 and 4 months appear. This evolution points to a general intensification and diversification of short-term variability, consistent with broader changes in the regional climate regime (Zolina et al. 2010).

Spectral density estimates computed from series detrended using a linear Holt–Winters model and centered moving averages (36-month window) are reported in the Supplementary Materials (Figures S1 and S2). Table S1 reports the optimized smoothing parameters, α (level) and β (trend), which determine the weight assigned to recent observations relative to historical data in the estimation of the trend component. Values of α or β approaching 1 indicate a reactive model, in which the estimates are strongly influenced by the most recent observations and are therefore more sensitive to sudden changes. Conversely, values approaching 0 indicate a more stable and conservative model, in which the estimates are smoothed over a longer time horizon and short-term fluctuations are dampened. In this study, the optimized values for the *LTrange* and *P* series suggest a relatively stable model structure, indicating that the underlying dynamics of these time series remain broadly consistent over time. In contrast, the optimized values for the *LTmin*, *LTmax, LTmean,* and *LC* series indicate a more reactive model behavior, suggesting that these variables are characterized by more frequent or pronounced temporal changes. Prior to spectral analysis, the detrended series were tested using Fisher's Kappa and Bartlett's Kolmogorov–Smirnov tests. For both detrending approaches, the results indicated significant departures from a white-noise spectrum in most cases with the sole exception of Fisher's Kappa test for precipitation depth, which did not provide strong evidence to reject the null hypothesis of white noise. To assess the assumption of homoscedasticity, the Breusch–Pagan and White tests were also applied. In all cases, the tests yielded *p*-values greater than 0.1, indicating no statistically significant evidence of heteroscedasticity.

The comparison among the three preprocessing methods (first differencing, Holt–Winters decomposition, and moving averages) indicates that the main conclusions are qualitatively robust across detrending approaches. The results for the *LC* series remain nearly unchanged across all methods. For precipitation (*P*), both the Holt–Winters decomposition and moving-average methods reveal a new peak at 12 month, which shifts to 12.5 in the most recent 23-year interval. For *LTmin*, *LTmax*, and *LTmean*, the Holt–Winters detrending approach identifies an additional spectral peak at the 6-month period, whose intensity varies over the same 23-year period. These features highlight subtle differences in the temporal structure of these series. In the *LTrange* series, both alternative methods primarily indicate an amplification of the 6-month and 12-month spectral peaks, without evidence of additional dominant periodic components at other frequencies. This discrepancy among methods is explicitly acknowledged and presented as a methodological limitation of the analysis.

Table 3 reports the squared coherence and phase (expressed in months) between the CO_2 series and the other climatic variables for the full period 1979–2024. Only periods shorter than 137 months are shown, corresponding to spectral estimates based on more than eight independent segments. The choice of eight segments follows established practices in spectral estimation to ensure an optimal trade-off between frequency resolution and variance reduction (Bendat and Piersol 2011; Priestly, 1981). This configuration provides approximately 15 degrees of freedom, which is widely considered the minimum threshold to achieve statistically stable estimates in geophysical time series analys (Emery and Thompson, 2001).

The *p*-values of Fisher's Kappa and Bartlett's Kolmogorov–Smirnov tests are below 0.0001 for all first-differenced series over the full period, with the exceptions of Fisher's Kappa test for *LTrange* ($p = 0.08$) and for precipitation depth ($p = 0.012$). Considering coherence as a squared correlation coefficient depending on frequency (Von Storch and Zwiers 2003) values ≥ 0.6 are generally interpreted as indicating a strong correlation (Schober et al. 2018). Values ≥ 0.6 which are consistently observed across comparable periods and suggest a stable relationship between the corresponding time series are highlighted in bold.

All temperature-related time series exhibit strong coherence with CO_2 at the 12–13-month period. Negative phase values indicate that variations in CO_2 precede changes in temperature, with effects appearing approximately one month earlier for *LTmin*, *LTmax*, and *LTmean*, and about 2.5 months earlier for *LTrange*. Correlation at the annual period may partly reflect shared seasonality, and the observed phase differences could therefore be influenced by shifts in seasonal patterns. For all temperature series, the phase is generally negative for correlations highlighted in bold at periods shorter than 18 months (i.e., less than approximately one and a half years), whereas it becomes positive at longer periods. This behavior suggests a scale-dependent relationship: over shorter timescales, variations in CO2 tend to

Table 3 Summary results of the cross-spectral analysis between local CO_2 (*LC*) and local climatic variables, including minimum temperature (*LTmin*), maximum temperature (*LTmax*), mean temperature (*LTmean*), temperature range (*LTrange*), and precipitation depth (*P*). The parameter γ2 denotes the squared coherence between each pair of time series

Period in months	$\gamma^2 LC$ and *LTmin*	Phase in months	$\gamma^2 LC$ and *LTmax*	Phase in months	$\gamma^2 LC$ and *LTmean*	Phase in months	$\gamma^2 LC$ and *LTrange*	Phase in months	$\gamma^2 LC$ and *P*	Phase in months
137.0	0.54	22.0	**0.62**	15.0	**0.74**	4.3	0.18	-24.9	0.15	12.0
109.6	0.61	18.0	**0.67**	17.0	**0.70**	9.8	0.08	21.6	0.12	13.3
91.3	0.24	13.4	**0.70**	15.0	**0.70**	11.5	0.07	18.1	0.21	5.6
78.3	0.20	1.9	**0.64**	8.0	**0.61**	5.6	0.25	13.0	0.32	11.2
68.5	0.51	2.1	**0.67**	4.6	**0.70**	2.4	0.12	11.7	**0.59**	14.6
60.9	0.61	4.2	0.38	4.6	0.49	3.9	0.02	0.7	**0.76**	12.8
54.8	0.49	6.6	0.15	5.9	0.31	6.1	0.03	9.0	**0.68**	9.8
49.8	0.44	10.4	0.02	8.4	0.12	7.9	0.05	12.3	0.36	4.3
45.7	0.55	9.6	0.10	-9.0	0.15	8.7	0.05	0.6	0.52	-3.3
42.2	0.35	8.8	0.30	-7.4	0.38	8.6	0.23	-3.5	0.59	-3.9
39.1	0.12	-8.4	0.40	-5.9	0.35	9.2	0.24	-4.0	0.41	-2.4
36.5	0.16	-6.8	0.29	-2.6	0.29	-7.4	0.09	2.7	0.35	0.0
34.3	0.39	-8.4	0.18	-3.9	0.40	-7.4	0.13	5.0	0.28	-1.8
32.2	0.63	7.3	0.42	-6.1	0.61	7.4	0.11	0.1	0.28	-6.8
30.4	0.51	7.4	0.49	-5.1	0.33	-7.6	0.37	-2.1	0.45	7.6
28.8	0.30	7.1	0.44	-4.5	0.18	-6.6	**0.65**	-1.7	0.47	-6.9
27.4	0.48	6.7	0.46	-4.9	0.38	-6.6	**0.65**	0.9	0.35	-6.2
26.1	0.63	6.2	0.55	-5.0	0.68	6.5	**0.71**	2.3	0.13	5.2
24.9	0.58	5.6	0.56	-4.2	**0.72**	6.1	0.58	1.8	0.01	-2.4
23.8	0.54	4.2	0.54	-4.5	**0.65**	5.1	0.48	0.0	0.29	-0.2
22.8	**0.70**	4.8	0.73	-5.1	**0.70**	5.1	0.38	-1.6	0.51	0.2
21.9	**0.75**	4.5	0.42	5.2	**0.64**	4.7	0.10	1.4	0.49	2.5
21.1	**0.78**	3.9	0.05	4.0	0.51	4.0	0.43	3.8	0.66	3.8
20.3	**0.79**	3.7	0.00	2.8	0.40	3.8	0.59	3.6	0.49	3.8
19.6	**0.64**	4.2	0.11	-2.6	0.40	4.5	0.33	2.5	0.15	-0.2
18.9	0.52	-3.4	0.49	-2.8	0.57	-4.0	0.16	-1.0	0.61	-2.6
18.3	**0.70**	-2.2	**0.64**	-2.2	**0.71**	-3.0	0.00	3.9	0.46	-3.2
17.7	**0.82**	-1.7	**0.67**	-1.7	**0.87**	-2.3	0.11	-1.7	0.21	4.4
17.1	**0.72**	-1.5	**0.61**	-2.0	**0.92**	-1.9	0.05	1.0	0.07	-0.3
16.6	0.56	-1.7	0.56	-1.6	**0.86**	-1.8	0.03	-1.1	0.21	-3.9
16.1	0.49	-2.5	0.58	-1.0	**0.65**	-1.7	0.18	1.1	0.26	2.9
15.7	0.45	-2.2	**0.70**	-0.8	0.51	-1.5	0.29	1.6	0.34	2.0
15.2	**0.66**	-1.2	**0.88**	-1.3	**0.77**	-1.7	0.10	-1.9	0.34	1.6
14.8	**0.73**	-1.0	**0.91**	-1.8	**0.86**	-2.0	0.48	-3.6	0.38	0.6
14.4	0.47	-1.7	**0.87**	-2.3	**0.76**	-2.5	0.66	-3.0	0.57	0.0
14.1	0.42	-2.3	**0.83**	-2.3	**0.68**	-2.6	0.58	-2.3	0.25	-0.5
13.7	0.50	-1.5	**0.81**	-1.8	**0.66**	-1.8	0.51	-2.4	0.20	-3.2
13.4	**0.73**	-1.2	**0.86**	-1.7	**0.82**	-1.5	0.58	-3.1	0.36	2.8

Table 3 (continued)

Period in months	γ^2LC and *LTmin*	Phase in months	γ^2LC and *LTmax*	Phase in months	γ^2LC and *LTmean*	Phase in months	γ^2LC and *LTrange*	Phase in months	γ^2LC and *P*	Phase in months
13.0	**0.87**	-1.0	**0.88**	-1.4	**0.89**	-1.3	0.55	-3.2	0.00	-2.5
12.7	**0.97**	-0.9	**0.94**	-1.1	**0.95**	-1.0	**0.63**	-2.8	0.04	2.0
12.5	**0.99**	-0.9	**0.99**	-1.1	**0.99**	-0.9	**0.89**	-2.6	0.09	1.6
12.2	**0.99**	-0.8	**0.99**	-1.1	**0.99**	-0.9	**0.97**	-2.5	0.32	1.2
11.9	**0.99**	-0.8	**0.99**	-1.0	**0.99**	-0.9	**0.98**	-2.4	0.46	1.0

precede temperature changes, while over longer timescales temperature variations appear to lead changes in CO2. This pattern is plausible in a localized urban context. Microclimatic processes and longer-term urban effects may differentially influence the temporal dynamics of temperature and CO_2. High coherence values ($\gamma 2 \geq 0.60$), consistent across adjacent frequency bands and indicative of a robust linear relationship between local CO_2 concentrations and temperature with negative phase, are observed at the following periods: 15, 17–18 months for *LTmin*; up to 18 months for *Ltmax* and *LTmean*.

Coherence values exceeding 0.60 with a positive phase are also detected at longer periods, including 20–23 months for *LTmin* (with minimum temperature preceding CO_2 by 4–5 months), 23–25 months for *LTmean* (with mean temperature preceding CO_2 by approximately 5–6 months), and around 27–28 months for *LTrange* (with temperature range alternatively leading or lagging CO_2 by about one or two months). In addition, *LTmax* and *LTmean* show coherence with CO_2 over periods of 68–137 months (approximately 6–11 years). At these scales, temperature precedes CO2 variations. However, the reliability of these long-period estimates decreases as the number of independent segments diminishes. For example, coherence at 137 months is based on only eight segments, compared with 92 segments available at the 12-month period. The squared coherence analysis does not reveal any statistically meaningful relationship between CO_2 and precipitation depth, except for weak signals at approximately 55 and 61 months, where precipitation appears to lead CO_2 by about 10 and 13 months. Overall, the results indicate that CO_2 concentrations are not systematically correlated with precipitation depth across the examined frequency range. In contrast, the relationship between local CO_2 and temperature is characterized by strong coherence at periods shorter than 18 months, where CO_2 leads temperature. At longer periods, the apparent direction of influence is reversed. This spectral evidence suggests a leading role of temperature variability at interannual timescales. It is consistent with a dominant role of climate variability in shaping CO_2 fluctuations. This interpretation is consistent with findings from atmospheric inversion studies (e.g., Rödenbeck et al. 2018), which show that interannual anomalies in CO2 fluxes are primarily driven by climate variability, with temperature commonly serving as a proxy for climatic forcing. The agreement between the spectral results and inversion-based evidence reinforces the conclusion that temperature-mediated processes play a dominant role in controlling interannual CO_2 dynamics.

Coherences computed from series detrended using a linear Holt–Winters model and centered moving averages (36-month window) are reported in the Supplementary Materials (Tables S2 and S3). The main results of the previously

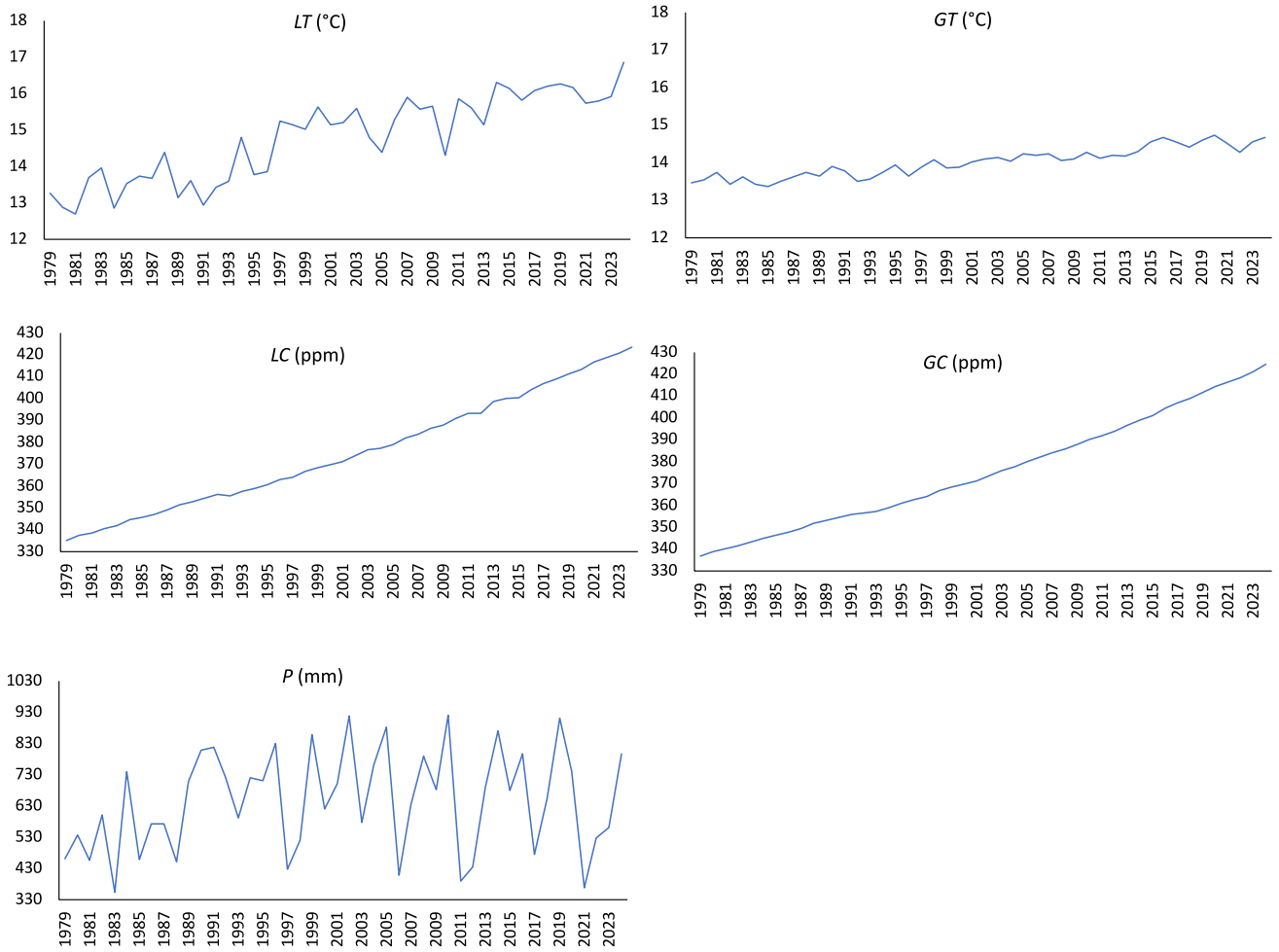

Fig. 3 Annual time series of local mean temperature (*LT*), global mean temperature (*GT*), local CO_2 (*LC*), global CO_2 (*GC*), and local precipitation depth (*P*) used in the analysis

reported coherence analysis are confirmed to be robust, as the same patterns are observed when applying these alternative preprocessing methods. While the overall coherence structures remain consistent across the three detrending approaches, estimated phase lags may exhibit slight variations, typically within a range of a few months for shorter periods and several months for longer periods. Major differences in coherence estimates are detected only at periods exceeding 50 months. This behavior was expected and is considered potentially unreliable given the limited number of segments available for coherence estimation at such low-frequency scales. Notably, all methods indicate that CO_2 concentrations are not systematically correlated with precipitation depth across the examined frequency range, with the sole exception of a possible correlation around 60 months, which is consistently detected by all three methods.

Table 4 Summary results of the Mann–Kendall and von Neumann trend tests

Series	Mann–Kendall trend test		von Neuman test
	p-value	Sen's slope	*p*-value
LT (°C)	**<0.0001**	0.076	**<0.0001**
GT (°C)	**<0.0001**	0.027	**<0.0001**
LC (ppm)	**<0.0001**	1.918	**<0.0001**
GC (ppm)	**<0.0001**	1.913	**<0.0001**
P (mm)	0.0860	3.089	0.3720

3.2 Annual series

Annual series of local mean temperature (*LT*), global mean temperature (*LG*), local CO_2 (*LC*), global CO_2 (*GC*), and local precipitation depth (*P*) are shown in Fig. 3.

Summary results of the Mann–Kendall (MK) and von Neumann tests are reported in Table 4. The results indicate that both local and global temperature, as well as local and global CO_2 concentrations, exhibit statistically significant deterministic linear trends. Specifically, local

temperature (*LT*) increases at a rate of 0.076 °C yr^{-1}, while global temperature (*GT*) shows an average increase of 0.027 °C yr^{-1}. Similarly, local CO_2 concentrations increase by 1.918 ppm yr^{-1}, slightly exceeding the global CO_2 growth rate of 1.913 ppm yr^{-1}. Consistent with the behavior observed in the monthly series, annual precipitation depth does not exhibit a statistically significant trend over the study period. This result agrees with several studies reporting the absence of a clear or univocal trend in total precipitation depth in Italy (e.g., Caporali et al. 2021).

Summary results of the Pettitt, Buishand, and SNHT tests for shifts in central tendency are reported in Table 5. The results of all three tests consistently support the presence of non-stationarity in local temperature (*LT*), global temperature (*GT*), local CO_2 (*LC*), and global CO_2 (*GC*). For local precipitation, all tests identify the same change point, occurring in 1996, whereas for the other series the estimated breakpoints differ only slightly. Overall, the tests consistently reject the null hypothesis of a constant location parameter over time for all variables except precipitation.

Notably, for both local and global CO_2, the detected change points either coincide or differ by no more than one year across all tests, indicating a robust signal of structural change. The change points identified in this analysis represent times at which the annual behavior of the climatic series undergoes a statistically significant shift. In the presence of a positive linear trend, these breakpoints correspond to marked changes in the average annual rate of increase.

By contrast, the change points previously identified in the monthly series reflect modifications in the intra-annual dynamics of the variables, in addition to those observed at the annual scale. Together, these results suggest that climate-related changes manifest not only as long-term trends but also as alterations in seasonal and sub-annual variability.

When comparing local and global variables, variations in local temperature trends are observed to precede those in global temperature, whereas local and global CO_2 concentrations appear to evolve synchronously. To assess interannual variability, spectral analysis was applied to the first-difference series. Additional tests performed on the differenced data (not reported here for brevity) confirmed the absence of trends and structural breaks in these series. The assumption of homoscedasticity was evaluated by applying the Breusch–Pagan and White tests to the residuals of the regression model. In all cases, the tests yielded *p*-values greater than 0.1, indicating no statistically significant evidence of heteroscedasticity. For the annual series, given their short length, we complemented the White and Pagan tests with a graphical analysis of the residuals. This confirmed the absence of heteroscedasticity, and the corresponding plots are provided in the Supplementary Materials (Figure S3).

Spectral density estimates obtained using quadratic kernel smoothing are shown in Fig. 4. Comparable spectral shapes were obtained when using Truncated, Parzen, Bartlett, and Tukey–Hanning kernels.

The global temperature series is characterized by the absence of pronounced interannual periodicities, apart from the strong linear trend identified in previous analyses. In contrast, the local temperature series exhibits distinct periodic components with cycles of approximately 2 and 3 years. These results are consistent with the spectral energy distribution observed across Mediterranean and European regions, where significant temperature variability has been documented at similar interannual scales, specifically around the 2.1-year and 4.2-year marks (Siarkos and Sen 2020). Spectral analysis of series detrended using Holt–Winters decomposition and a 3-year moving average confirms these results, also indicating a possible additional periodic component for *LT* at approximately 16 years (Holt–Winters). Spectral densities are reported in Supplementary Materials (Figures S4 and S5).

The increase in spectral density toward longer periods (lower frequencies) observed in both local and global CO_2 series is indicative of red-noise–like behavior, commonly associated with persistent autocorrelation or residual non-stationarity. These features likely reflect low-frequency variability rather than genuine periodic components. An opposite behavior (i.e., enhanced high-frequency variability) is observed in the spectra obtained using the Holt–Winters method, whereas the moving-average method does not exhibit comparable features at low frequencies. Although the annual local and global CO_2 series appear very similar in magnitude and overall temporal evolution, and their Sen's slope estimates of annual growth rates (Table 4) are nearly identical, their interannual behavior differs substantially when examined in the frequency domain. The global CO_2 series exhibits only weak spectral peaks at periods shorter

Table 5 Summary results of the Pettitt's and Buishand's tests

	Pettitt's test		Buishand's test		SNHT test	
Series	*p*-value	*t*	*p*-value	*t*	*p*-value	*t*
LT(°C)	**<0.0001**	1996	**<0.0001**	1996	**<0.0001**	1996
GT (°C)	**<0.0001**	2001	**<0.0001**	2000	**<0.0001**	2000
LC (ppm)	**<0.0001**	2001	**<0.0001**	2002	**<0.0001**	2005
GC (ppm)	**<0.0001**	2001	**<0.0001**	2002	**<0.0001**	2004
P (mm)	0.2270	1988	0.1030	1988	0.0650	1988

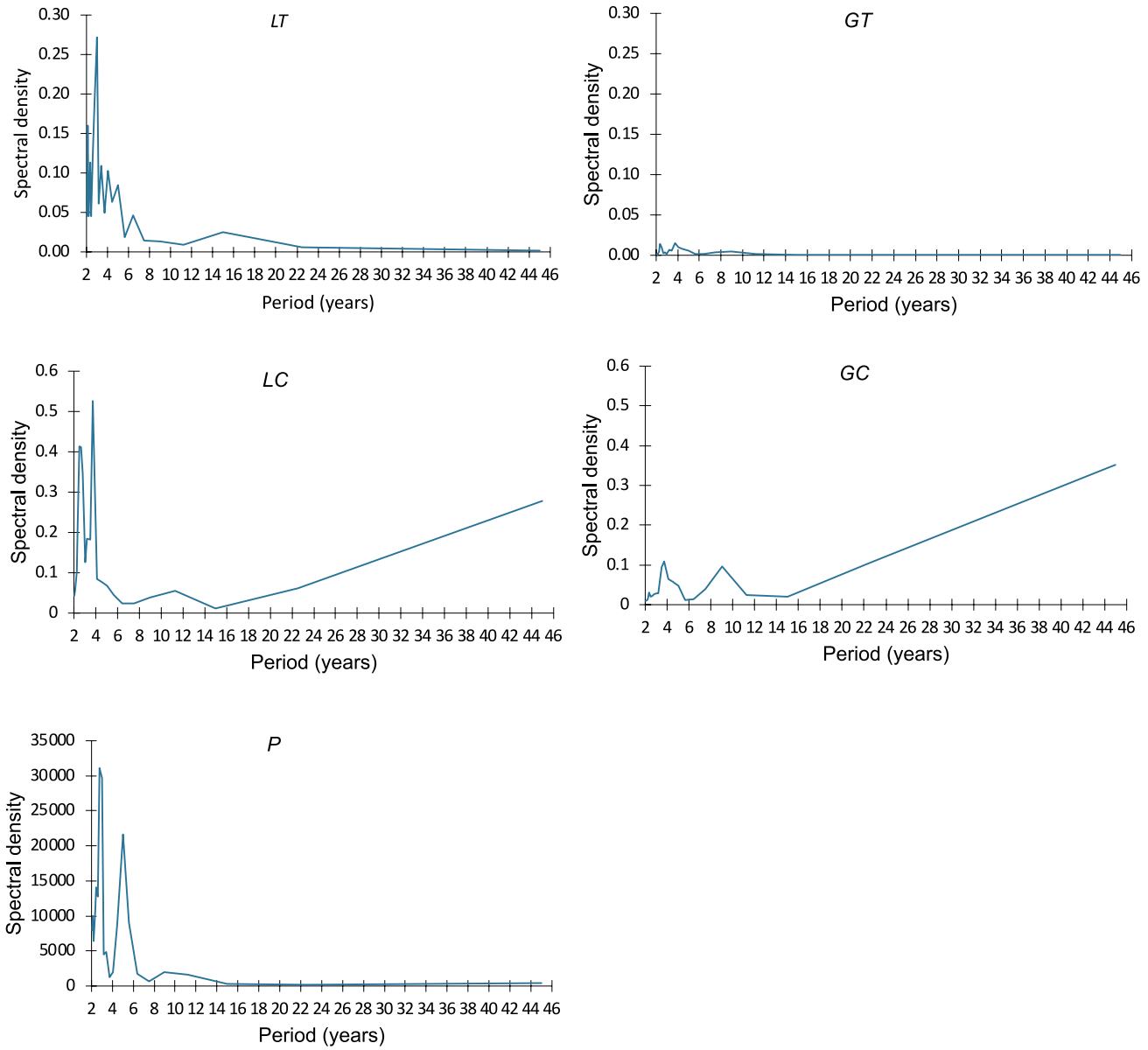

Fig. 4 Spectral density estimates of the annual time series of local mean temperature (*LT*), global mean temperature (*GT*), local CO_2 (*LC*), global CO_2 (*GC*), and local precipitation depth (*P*) over the period 1979–2024

than 9 years, whereas the local CO_2 series displays more pronounced peaks near 2.5 and 3.5 years, indicating stronger cyclical variability at the local scale. These results are consistent across all three methods.

Precipitation depth shows dominant spectral peaks at approximately 3 and 5-year periods. Consistent with the analysis of historical climate series in Italy by Brunetti et al. (2006), these findings highlight the prevalence of interannual cycles in regional precipitation. Furthermore, the sharpness of these peaks suggests the superior frequency resolution of the Fourier transform compared to dyadic wavelet decompositions, which tend to average spectral energy over broader frequency bands. The robustness of this result is further confirmed by its consistent reproduction across all three detrending approaches.

The presence of relatively short-period cyclic components in local climatic variables may reflect changes in underlying climate variability, potentially linked to recent climate change. Overall, these results indicate that the variance of mean temperature and precipitation can evolve over decadal or even shorter timescales. They further support the growing evidence that, at the local scale and over recent decades, traditional climate definitions based on fixed 30-year normals are increasingly inadequate. Instead, decadal or shorter averaging periods are becoming more

Table 6 Summary results of the cross-spectral analysis between global CO_2 and local temperature (*GC/LT*), local CO_2 and local temperature (*LC/LT*), local precipitation depth and local temperature (*P/LT*), global temperature and local temperature (*GT/LT*), and global CO_2 and local CO_2 (*GC/LC*). γ^2 denotes the squared coherence

Period (years)	γ^2*GC and LT*	Phase (years)	γ^2*LC and LT*	Phase (years)	γ^2*P and LT*	Phase (years)	γ^2*GT and LT*	Phase (years)	γ^2*GC and LC*	Phase (years)
5.0	**0.85**	-1.29	**0.83**	-0.81	**0.83**	1.14	**0.66**	0.29	0.57	0.88
4.5	**0.81**	-0.98	**0.63**	1.56	0.32	-0.34	0.54	-0.13	0.52	-1.45
4.1	**0.80**	-1.35	0.05	-0.33	0.37	0.03	0.79	-0.10	0.10	1.43
3.8	0.50	0.55	0.40	0.14	0.28	0.99	0.52	-1.42	0.88	1.35
3.5	**0.83**	-0.62	0.48	1.55	**0.97**	0.16	0.55	1.06	0.34	-1.15
3.2	0.03	-0.83	0.42	-1.49	**0.87**	-0.06	0.09	-1.30	0.74	0.05
3.0	0.64	0.76	**0.64**	-0.86	**0.93**	-0.28	0.37	0.58	0.19	1.11
2.8	0.53	-1.37	**0.85**	-1.54	**0.86**	-0.94	**0.82**	1.34	**0.88**	-0.12
2.6	0.83	1.03	**0.88**	1.26	**0.62**	-0.36	**0.65**	0.61	**0.67**	-0.87
2.5	0.31	-0.54	0.53	-0.83	0.06	0.42	0.49	0.98	**0.82**	1.45
2.4	0.85	0.58	0.83	-0.32	**0.72**	-0.02	**0.87**	-1.13	**0.84**	-0.90
2.3	0.05	-1.37	0.42	0.29	0.43	0.44	0.24	-0.32	**0.91**	-0.46
2.1	0.78	0.12	0.69	-0.14	**0.78**	1.54	0.29	-0.79	**0.63**	-0.33
2.0	0.54	0.86	0.15	-0.97	0.13	0.89	0.35	0.51	**0.65**	0.94

Table 7 Summary results of the cross-spectrum analysis between global CO_2 and local precipitation depth (*GC/P*), Local CO_2 and local precipitation depth (*LC/P*), global temperature and local precipitation depth (*GT/P*), global temperature and local CO_2 (*GT/LC*), global CO_2 and global temperature (*GC/GT*). γ^2 is the squared coherence

Period (years)	γ^2*GC and P*	Phase (years)	γ^2*LC and P*	Phase (years)	γ^2*GT and P*	Phase (years)	γ^2*GT and LC*	Phase (years)	γ^2*GC and GT*	Phase (years)
5.0	0.69	0.05	**0.89**	1.26	**0.83**	-1.02	0.57	0.88	**0.74**	0.82
4.5	0.29	-0.04	**0.81**	-1.17	0.48	0.89	0.52	-1.45	**0.76**	-0.64
4.1	0.41	-1.47	0.05	-1.14	0.33	-0.08	0.10	1.43	**0.96**	-1.19
3.8	**0.70**	-0.80	0.40	-1.19	0.54	0.33	0.88	1.35	**0.95**	-1.04
3.5	**0.89**	-0.81	0.59	1.31	0.53	0.83	0.34	-1.15	**0.78**	-1.49
3.2	0.04	0.61	0.12	-1.55	0.00	1.48	0.74	0.05	**0.65**	-1.09
3.0	**0.77**	-0.92	**0.74**	-0.49	0.26	0.99	0.19	1.11	0.21	0.00
2.8	**0.70**	-0.27	**0.85**	-0.59	0.71	-0.67	**0.88**	-0.12	**0.74**	0.23
2.6	0.38	1.13	0.44	1.37	0.09	1.19	**0.67**	-0.87	**0.63**	0.62
2.5	0.53	-0.82	0.55	-0.73	**0.62**	0.37	**0.82**	1.45	**0.88**	-1.37
2.4	0.63	0.71	0.40	-0.10	**0.71**	-0.92	**0.84**	-0.90	**0.86**	-1.35
2.3	0.24	-1.13	0.45	0.67	0.35	0.24	**0.91**	-0.46	0.29	0.60
2.1	0.52	1.51	**0.62**	1.43	0.16	1.18	**0.63**	-0.33	0.39	0.89
2.0	0.58	0.17	**0.80**	1.32	0.65	-0.90	**0.65**	0.94	0.57	0.81

relevant for characterizing present and near-future climate conditions (Speer and Leslie 2024; Speer et al. 2024; Srinivasan et al. 2024).

Tables 6 and 7 report the squared coherence and phase (expressed in years) for each pair of time series. Results are shown for periods shorter than 5 years, corresponding to estimates based on more than eight independent segments. Table S5 provided in the Supplementary Materials reports estimated parameters of the Holt-Winters model. Tables S5, S6, S7, and S8 report the coherences and phases obtained from series detrended using the Holt–Winters model and moving-average filtering. The highest coherence values ($\geq$0.60), observed at comparable periods and across different methods, are interpreted as indicative of a robust relationship between the corresponding time series and are highlighted in bold. For several pairs of variables (e.g., *GC–LT*, *LC–LT*, *P–LT*, *GC–P*, *LC–P*, *GT–P*, *GT–LC*, and *GC–GT*), the coherence and phase relationships may be interpreted as indicative of potential interdependencies among the variables. For other pairs (e.g., *GT–LT* and *GC–LC*), the analysis is intended primarily to identify shared periodic behavior, without implying any causal relationship.

Notably, the results indicate that at the global scale, CO_2 leads temperature by approximately one year at 3.2–4.5-year periods. Dominant periodicity among these variables is also observed at 5-year period, with phase exhibiting opposite signs. Correlations are also observed at 2.4–2.8-year period. These findings are consistent with the landmark study by Kuo et al. (1990), who established a high coherence between global CO_2 and temperature using a shorter

dataset (1958–1987). While Kuo et al. identified a lead-lag relationship reflecting the feedback between thermal anomalies and the carbon cycle, our results, extending to 2024, confirm that these strong interannual couplings persist and remain a robust feature of the global climate system even under the accelerated warming of recent decades.

Local temperature appears to be influenced by global CO_2 variability on a 4–5-year and 3.5-year timescale, with global CO_2 changes preceding local temperature fluctuations by roughly one year. In contrast, local temperature seems to lead local CO_2 variations on a 2.6-year and 4.5-year timescale while being affected by local CO_2 at 2.8–3-year and 5-year timescales, again with an approximate one-year lead. The 2.6-year periodicity identified in the annual dataset aligns consistently with the significant coherence peak (exceeding 0.6) observed at the 32.3-month scale in the monthly series (Table 3). The robustness of this cross-scale connection is further supported by the phase analysis, which reveals the same sign and a consistent lead-lag relationship across both temporal resolutions, suggesting a stable physical coupling at this inter-annual frequency. These specific periodicities, particularly in the 2–5 years range, align with the interannual climate variability characteristic of the North Atlantic sector, often associated with the North Atlantic Oscillation (Hurrell 1995; Hurrel & Van Loon, 1997). This suggests two distinct coupling mechanisms: first, that global CO_2 dynamics are coupled with large-scale atmospheric circulation patterns that modulate European temperature records; second, that regional temperature oscillations may trigger delayed responses in local CO_2 concentrations through mechanisms such as soil respiration and vegetation dynamics.

When examining annual values, a relationship between local CO_2 and local precipitation depth is observed at the 2-year and 2.8–3-year periods. Specifically, variations occur with a phase lead of approximately half a year and a lag of one to one-and-a-half years, respectively. Another relationship emerges at the 4.5–5-year timescale, where local CO_2 alternately leads or lags precipitation depth by about one year. This alternating lead-lag behavior at longer periods may reflect the complex feedback mechanisms between regional soil moisture availability and carbon sequestration capacity. The 5-year periodicity identified in the annual dataset align with the significant coherence peak (exceeding 0.6) observed at the 60.9-month scale in the monthly series. Additionally, global CO_2 is correlated with local precipitation at the 2.8–3-year period and at the 3.5–3.8-year period, leading local precipitation by roughly one year.

Local precipitation depth is correlated with global temperature only at the 5-year and 2.5-year periods. In addition, local temperature and precipitation depth display coherent variability at the 2.6–3.5-year and 5-year timescale, suggesting the presence of a shared mode of interannual variability.

No robust evidence of persistent common periodic patterns is observed between local and global temperature series. Although relatively high squared coherence values appear at timescales of approximately 2.6–2.8 years and around 5 years, these features are not consistently supported across adjacent periods (e.g., 2.5 or 3.0 years), suggesting that the apparent coherence may not be structurally stable. In contrast, the global and local CO_2 series exhibit a more consistent pattern of shared variability, particularly within the 2.0–2.8-year timescale, indicating clearer evidence of common dynamics at this frequency range.

Across the various detrending techniques, the estimated phases of the coherences discussed above, which remain reasonable consistent across all detrending methods, show a certain degree of stability, with inter-method discrepancies confined to a sub-annual window of approximately 0 to 7 months.

Overall, the results indicate that both global and local CO_2 concentrations are associated with local climatic variables, specifically mean annual temperature and total precipitation depth, across multiple interannual timescales. Global CO_2 is more consistently associated with variations in local temperature and precipitation, whereas local CO_2 exhibits more complex behavior, alternately leading or lagging temperature and precipitation depending on the characteristic timescale of the oscillation. Global and local CO_2 show similar variability at timescales shorter than three years. Finally, annual values of local temperature and precipitation depth exhibit interannual relationships at periods shorter than three and a half years, in contrast to monthly values, which are dominated by strong seasonal variability.

4 Discussion

The results of this multi-scale interaction study show that climate variability in the Modena urban area is structured across multiple temporal scales, with distinct mechanisms operating at seasonal and interannual frequencies (Sect. 3; Figs. 2 and 4). Spectral analysis confirms that temperature retains a highly stable annual cycle, whereas precipitation depth and temperature range exhibit marked changes in intra-annual variability over the last two decades (Sect. 3.1; Fig. 2). This divergence suggests that climate change in urban environments may manifest less through disruption of mean seasonal temperature cycles and more through altered variability, extremes, and short-period fluctuations (Sect. 3.1). The emergence of additional short-period components in precipitation (2–4 months) and temperature range (6-month) after 2001 is particularly noteworthy (Sect. 3.1; Fig. 2). Such behavior is consistent with a reorganization of atmospheric circulation patterns and moisture transport, as

documented in other European regions, and implies increasing intermittency rather than monotonic change. Temperature range appears especially sensitive to these shifts, reinforcing its value as an indicator of local climate instability and urban heat island dynamics (Sect. 3.1; Fig. 2).

Cross-spectral analysis reveals that relationships between CO_2 and climatic variables are strongly scale dependent (Sect. 3; Tables 3, 6, and 7). At the seasonal scale, the strong coherence between local CO_2 and temperature, with CO_2 leading temperature, likely reflects shared seasonal forcing, including biospheric uptake and anthropogenic emission cycles (Sect. 3.1; Table 3). However, at interannual timescales, the phase relationships reverse more frequently, with temperature variability often preceding changes in CO_2 (Sect. 3.2; Tables 6 and 7). This behavior supports the interpretation that climate variability acts as a driver of interannual CO_2 anomalies rather than the reverse, in agreement with atmospheric inversion studies linking CO_2 flux variability to temperature-controlled ecosystem processes. The identified scale-dependent phase relationships suggest the presence of different dominant processes operating at different temporal scales. At shorter timescales, the apparent leading role of CO_2 may reflect large-scale atmospheric variability. In this context, CO_2 acts as a background tracer of circulation and biospheric dynamics that influence local temperature. At longer timescales, this relationship appears to reverse, with temperature leading CO_2 variability. This behavior may be associated with local and regional processes, including thermal inertia, land–atmosphere feedbacks, and urban microclimatic effects such as heat storage and release within the built environment. These processes can enhance temperature persistence. In turn, they may influence atmospheric CO_2 through biospheric and surface–atmosphere exchange. While these interpretations provide a physically consistent framework, they remain indicative, as the present analysis is based on statistical relationships and does not establish causal mechanisms. Overall, the results highlight a consistent framework for distinguishing between relationships driven by shared seasonal variability and those emerging at interannual scales.

At intra-annual timescales, precipitation is primarily driven by atmospheric circulation and moisture transport, while local CO_2 is influenced by mixing processes and biospheric activity. At these frequencies, no significant relationship is observed between the two variables. At intermediate scales, variability is linked to shifts in circulation regimes and precipitation intermittency, and the analysis reveals weak or shifting phase relationships. Global CO_2 exhibits coherence at periods of approximately 3–3.5 years, while local CO_2 shows a similar behavior around 3 years. In these cases, CO_2 appears to lead, although this may reflect shared atmospheric drivers, with CO_2 acting as a background signal rather than a direct forcing. In addition, local CO_2 shows a correlation at the 2-year period (observed only in annual data), with a reversed phase relationship. At longer timescales (4.5 years and beyond), a more consistent relationship emerges in both monthly and annual data. Precipitation leads CO_2 at the 5-year period and lags CO_2 at the 4.5-year period. At these scales, precipitation variability is associated with large-scale climate patterns. CO_2 variability instead reflects broader biospheric and surface–atmosphere exchange processes. This alternating lead–lag behavior highlights the fundamentally different nature of the two variables: precipitation is characterized by intermittent, event-driven dynamics, while CO_2 represents a smoother and more integrative atmospheric signal. These interpretations remain indicative, as the analysis is based on statistical relationships and does not establish causality. A limitation of this approach lies in the use of a reconstructed global temperature series referenced to local baseline conditions. While this enables direct comparison with local observations, it does not capture regional deviations from global temperature patterns. Consequently, the inferred global–local relationships should be interpreted as interactions between local variables and large-scale background variability, rather than as evidence of direct physical coupling at the site level.

Differences between local and global CO_2 behavior further emphasize the importance of spatial scale. Although local and global CO_2 exhibit nearly identical long-term growth rates, their spectral signatures differ substantially, with local CO_2 showing stronger and shorter interannual periodicities (Sect. 3.2, Fig. 4). This suggests that regional processes, such as urban emissions, boundary-layer dynamics, and regional biospheric exchange, superimpose additional variability on the global signal. In contrast, global temperature exhibits limited coherent interannual structure, reinforcing the idea that local climate variability cannot be inferred directly from global averages (Sect. 3.2; Figs. 3 and 4).

Overall, the results highlight that apparent climate-carbon relationships depend critically on temporal aggregation and frequency (Sects. 3.1 and 3.2; Tables 3, 6, and 7). Relationships that are weak or ambiguous in the time domain become clearer when resolved spectrally, while others dissolve once shared seasonality is removed (Sect. 3; Figs. 1 and 3; Tables 1, 2, 4, and 5). This underscores the value of frequency-domain approaches for disentangling physical coupling from coincident variability in climate time series. The results presented in this study show robustness across the different analytical frameworks. However, certain findings should be interpreted with caution due to discrepancies observed among the three detrending methods. Specifically, divergence was noted in the coherence between *LC* and *LTmin* for cycles exceeding 50 months, as well as in the

spectral peaks of *LTrange* for high-frequency cycles shorter than 6 months. Additionally, variations in phase estimates across methods suggest a need for careful consideration when assessing precise temporal alignments.

Regarding gap-filling procedures, it is recognized that they may influence spectral estimates, particularly at higher frequencies. However, the limited extent of missing data in the monthly *LC* series ensures consistency of results across alternative interpolation methods, such as linear and cubic spline interpolation. This suggests that the main findings are robust to the treatment of missing values. Figure S6, provided in the supplementary materials, reports the spectral density (in the 2–14 months range) obtained with different preprocessing methods and missing value imputations and shows that the main peaks remain stable and the overall density remains largely unchanged.

While we acknowledge that Fourier analysis does not explicitly resolve transient or time-evolving frequency shifts, the choice of a Fourier-based framework is supported by a comparative assessment with alternative time–frequency methods. In a previous study (Morlini et al. 2023), a wavelet-based approach was employed to investigate temperature and precipitation series. However, a comparison between those previous findings and the result of the current study suggests that the Fourier framework offers a more straightforward and physically interpretable representation of the spectral and cross-spectral features. By avoiding the rigid dyadic scale partitioning of discrete wavelets, we were able to achieve a finer frequency localization, which is essential for precisely identifying the phase relationships of the specific periodicities discussed herein, with the assumption that results should be interpreted as representing dominant quasi-stationary components over the analysis period.

5 Conclusions

This study applied spectral and cross-spectral analysis to long-term temperature, precipitation, and CO_2 records to investigate scale-dependent climate–carbon interactions in an urban environment (Figs. 1 and 3). The results show that while local temperature maintains a stable seasonal cycle, precipitation depth and temperature range exhibit increasing short-period variability over the last two decades, indicating a reorganization of local climate variability rather than uniform trend amplification (Fig. 2). Strong coherence between CO_2 and temperature at the annual scale reflects shared seasonal forcing, whereas interannual relationships reveal a predominantly climate-driven control on CO_2 variability, with temperature frequently leading CO_2 fluctuations (Tables 3, 6, and 7). This behavior is consistent with climate-mediated modulation of carbon fluxes and highlights the limited explanatory power of CO_2 alone for interpreting local climate variability.

Despite similar long-term trends, local and global CO_2 exhibit distinct interannual dynamics, highlighting the role of regional processes in shaping urban-scale climate signals (Figs. 3 and 4). No robust interannual coupling is detected between local and global temperature, reinforcing the need to distinguish global forcing from local responses (Table 6). Taken together, these findings show that climate–carbon interactions are inherently scale dependent and that spectral methods provide critical insight beyond conventional trend analyses (Figs. 2 and 4). The results also suggest that fixed climatological normals may be insufficient to fully characterize present-day climate conditions, particularly in urban environments where variability evolves on decadal and sub-decadal timescales (Fig. 4). Finally, the identification of scale-dependent phase reversal provides a framework for distinguishing between relationships driven by shared seasonal forcing and those emerging at interannual scales, highlighting the risk of inferring climate–carbon relationships from time-domain analysis alone.

Supplementary Information The online version contains supplementary material available at https://doi.org/10.1007/s00477-026-03280-5.

Acknowledgements Air temperature and precipitation time series for Modena were provided by the Osservatorio Geofisico di Modena, Italy. Time series of local atmospheric CO2 concentrations were obtained from the Monte Cimone Observatory, a strategic site of the Italian Air Force Meteorological Service. The authors are grateful to Luca Lombroso and Giulio Paolini for his specific comments and feedback on these data. This research was supported by Fondazione Cassa di Risparmio di Modena (grant 2018-0093), the University of Modena and Reggio Emilia (grant FAR 2020 Mission Oriented), and the European Union NextGenerationEU/NRRP, Mission 4 Component 2 Investment 1.5, Call 3277 (12/30/2021), Award 0001052 (06/23/2022), under the project ECS00000033 'Ecosystem for Sustainable Transition in Emilia-Romagna,' CUP E93C2200110001, Spoke 6 'Ecological Transition Based on HPC and Data Technology.' The authors thank three anonymous reviewers for comments that led to improvements in the manuscript.

Author contributions Isabella Morlini and Stefano Orlandini contributed to the conception and design of the study. Material preparation, data collection, and analysis were conducted by both authors. The first draft of the manuscript was written by Isabella Morlini and Stefano Orlandini, who also reviewed and commented on previous versions. All authors have read and approved the final manuscript.

Funding Open access funding provided by Università degli Studi di Modena e Reggio Emilia within the CRUI-CARE Agreement. Fondazione Cassa di Risparmio di Modena,2018-0093,University of Modena and Reggio Emilia,FAR 2020 Mission Oriented,European Union NextGenerationEU/NRRP,Mission 4 Component 2 Investment 1.5,Call 3277 (12/30/2021),Award 0001052 (06/23/2022),under the project ECS00000033 'Ecosystem for Sustainable Transition in Emilia-Romagna,' CUP E93C2200110001,Spoke 6 'Ecological Transition Based on HPC and Data Technology.'

Data availability Data sets used in this study are available from the authors upon request.

Declarations

Conflict of interest The authors declare no competing interests.

References

Addinsoft (2023) XLSTAT Statistical and data analysis solutions. New York, USA. https://www.xlstat.com

Andrews DWK (1991) Heteroskedasticy and autocorrelation consistent covariance matrix estimation. Econometrica 59(3):817–858

Arizpe SS, Sánchez-Azofeifa A, Gamon JA, Portillo-Quintero C, Sharp I, Hird J (2021) Comparison of atmospheric CO_2 concentrations between urban and rural sites. Atmos Environ 244:117904

Bartlett MS (1967) Some remarks on the analysis of time-series. J Roy Stat Soc B 29(1):25–38

Bendat JS, Piersol AG (2011) Random data: analysis and measurement procedures, 4th ed. Wiley-Interscience, John Wiley & Sons, New York

Bharghavi K, Reddy TL, Kapa H et al (2025) Decadal analysis of monsoon climate variability and drought indicators in Rayalaseema: long-term analysis using satellite data and drought indices. Stoch Environ Res Risk Assess 39:4985–5009. https://doi.org/10.1007/s00477-025-03059-0

Bloomfield P (2000) Fourier analysis of time series: An introduction. John Wiley & Sons, New York

Breusch TS, Pagan AR (1979) A simple test for heteroscedasticity and random coefficient variation. Econometrica 47(5):1287–1294. https://doi.org/10.2307/1911963

Brunetti M, Maugeri M, Monti F, Nanni T (2006) Temperature and precipitation variability in Italy in the last two centuries from homogenous reconstructed series. Int J Climatol 26(3):345–381

Buishand TA (1982) Some methods for testing the homogeneity of rainfall records. J Hydrol 58:11–27

Buishand TA (1984) Tests for detecting a shift in the mean of hydrological time series. J Hydrol 73:51–69

Caporali E, Lompi M, Pacetti T, Chiarello V, Fatichi S (2021) A review of studies on observed precipitation trends in Italy. Int J Climatol 41:E1–E25

Costanzini S, Boccolari M, Vega Parra S, Despini F, Lombroso L, Teggi S (2024) A comparative analysis of temperature trends at Modena Geophysical Observatory and Mount Cimone Observatory, Italy. Int J Climatol 44:4741–4766

Cristofanelli P, Fierli F, Marinoni A, Calzolari F, Duchi R, Burkhart J, Stohl A, Maione M, Arduini J, Bonasoni P (2013) Influence of biomass burning and anthropogenic emissions on ozone, carbon monoxide and black carbon at the Mt. Cimone GAW-WMO global station (Italy, 2165 m a.s.l.). Atmos Chem Phys 13:15–30. https://doi.org/10.5194/acp-13-15-2013

Cristofanelli P, Guti´errez I, Adame J, Bonasoni P, Busetto M, Calzolari F, Putero D, Roccato F (2021) Interannual and seasonal variability of NOx observed at the Mt. Cimone GAW/WMO global station (2165 m a.s.l., Italy). Atmos Environ 249:118245. https://doi.org/10.1016/j.atmosenv.2021.118245

Cristofanelli P, Trisolino P, Calzolari F, Busetto M, Calidonna CR, Amendola S, Arduini J, Fratticioli C, Hundal RA, Maione M, Marcucci F, Marinoni A, Montaguti S, Renzi L, Roccato F, Bonasoni P, Putero D (2024) Influence of wildfire emissions to carbon dioxide (CO_2) observed at the Mt. Cimone station (Italy, 2165 m asl): a multi-year investigation. Atmos Environ 330:1205677. https://doi.org/10.1016/j.atmosenv.2024.120577

Douglas CM, Peck EA, Vining GG (2021) Introduction to linear regression analysis, 6th ed. Wiley

Emery WJ, Thomson RE (2001) Data analysis methods in physical oceanography. Elsevier

Esit M, Yuce MI, Yasa I, D IH (2025) Seasonal and annual precipitation characteristics of Türkiye and the influence of atmospheric-ocean interactions. Stoch Environ Res Risk Assess 39:4107–4124. https://doi.org/10.1007/s00477-025-03052-7

Fisher RA (1929) Tests of significance in harmonic analysis. Proc R Soc Edinb 49:1–16

Fuller WA (1976) Introduction to statistical time series. John Wiley & Sons

Gilbert RO (1987) Statistical methods for environmental pollution monitoring. Wiley, NY

Gogeri I, Gouda KC, Sumathy T (2024) Modeling and forecasting atmospheric carbon dioxide concentrations at Bengaluru city in India. Stoch Environ Res Risk Assess 38:1297–1312

Greene WH (2018) Econometric analysis, 8th ed. Pearson Education Limited, London

Haimberger L (2007) Homogenization of radiosonde temperature time series using innovation statistics. J Clim 20(7):1377–1403

Hipel KW, McLeod AI (1994) Time series modelling of water resources and environmental systems. Elsevier Science, New York

Holt CC (2004) Forecasting seasonals and trends by exponentially weighted moving averages. Int J Forecast 20(1):5–10

Hua L, Ma Z, Guo W (2008) The impact of urbanization on air temperature across China. Theor Appl Climatol 93(3):179–194

Hurrell JW (1995) Decadal trends in the North Atlantic Oscillation: regional temperatures and precipitation. Science 269(5224):676–679

Hurrell JW, Van Loon H (1997) Decadal variations in climate associated with the North Atlantic Oscillation. Clim Change 36:301–326

Hyndman RJ, Athanasopoulos G (2018) Forecasting: principles and practice. Otexts, Melbourne, Australia

Jenkins JM, Watts DG (1968) Spectral analysis and its applications. Holden-Day, San Francisco

Jevrejeva S, Moore JC, Grinsted A (2003) Influence of the Arctic Oscillation and El Niño-Southern Oscillation (ENSO) on ice conditions in the Baltic Sea: The wavelet approach. *Journal of Geophysical Research: Atmospheres*, 108(D21). https://doi.org/10.1029/2002JD002877

Kalnay E, Cai M (2003) Impact of urbanization and land-use change on climate. Nature 423(6939):528–531

Katavoutas G, Founda D, Varotsos KV, Giannakopoulos C (2023) Diurnal temperature range and its response to heat waves in 16 European cities – current and future trends. Sustainability 15:12715. https://doi.org/10.3390/su151712715

Kendal MG (1975) Rank correlation methods, 4th edition. Charles Griffin, London

Kivi R, Heikkinen P (2016) Fourier transform spectrometer measurements of column CO_2 at Sodankylä, Finland. Geosci Instrum

Method Data Syst 5:271–279. https://doi.org/10.5194/gi-5-271-2016

Kuo C, Lindberg C, Thomson DJ (1990) Coherence established between atmospheric carbon dioxide and global temperature. Nature 343(6260):709–714. https://doi.org/10.1038/343709a0

Lopes AM, Tenreiro Machado JAT (2018) Complexity analysis of global temperature time series. Entropy 20(6):437. https://doi.org/10.3390/e20060437

Mann HB (1945) Nonparametric tests against trend. Econometrica 13:163–171

Mann ME, Lees JM (1996) Robust estimation of background noise and signal detection in climatic time series. Clim Change 33:409–445

Morlini I, Orlandini S (2025) Anthropogenic heat effects on local deviations from the global mean annual air temperature: A case study of Modena, Italy. Stoch Environ Res Risk Assess. https://doi.org/10.1007/s00477-025-02990-6

Morlini I, Franco Villoria M, Orlandini S (2023) Modeling local climate change using site-based data. Environ Ecol Stat 30:205–232

Morlini I, Albertson S, Orlandini S (2024) Characterization of annual urban air temperature changes with special reference to the city of Modena: a comparison between regression models and a proposal for a new index to evaluate relationships between environmental variables. Stoch Environ Res Risk Assess 38:1163–1178. https://doi.org/10.1007/s00477-023-02622-x

Mumo L, Yu J, Ayugi B (2019) Evaluation of spatiotemporal variability of rainfall over Kenya from 1979 to 2017. J Atmos Sol-Terr Phys 194:105097. https://doi.org/10.1016/j.jastp.2019.105097

Nocedal J, Wright SJ (2006) Numerical optimization. Springer, New York

Olafsdottir KB, Schulz M, Mudelsee M (2016) REDFIT-X: cross-spectral analysis of unevenly spaced paleoclimate time series. Comput Geosci 91:11–18. https://doi.org/10.1016/j.cageo.2016.03.001

Percival DB, Walden AT (1993) Spectral analysis for physical applications. Cambridge Univ. Press

Pettitt AN (1979) A non-parametric approach to the change point problem. J R Stat Soc Ser C Appl Stat 28:126–135

Pili UB, Violanda RR (2020) Extracting Earth's orbital period from atmospheric CO_2 concentrations using the Fourier transform based on Matlab. Phys Educ 55(5):055001

Priestley MB (1981) Spectral analysis and time series. Academic Press, London

Rödenbeck C, Zaehle S, Keeling R, Heimann M (2018) How does the terrestrial carbon exchange respond to inter-annual climatic variations? A quantification based on atmospheric CO_2 data. Biogeosciences 15:2481–2498. https://doi.org/10.5194/bg-15-2481-2018

Sargent TJ (1987) Macroeconomic theory, 2nd ed. Academic Press, New York

Schober P, Boer C, Schwarte LA (2018) Correlation coefficients: appropriate use and interpretation. Anesth Analg 126(5):1763–1768

Sen PK (1968) Estimates of the regression coefficient based on Kendall's tau. J Am Stat Assoc 63:1379–1389

Shrestha S, Yao T, Adhikari TR (2019) Analysis of rainfall trends of two complex mountain river basins on the southern slopes of the Central Himalayas. Atmos Res 215:99–115. https://doi.org/10.1016/j.atmosres.2018.08.027

Siarkos I, Sen OL (2020) Wavelet analysis of precipitation and temperature over European regions. Theor Appl Climatol 140(3):1161–1180. https://doi.org/10.1007/s00704-020-03148-w

Speer M, Hartigan J, Leslie L (2024) The machine learning attribution of quasi-decadal precipitation and temperature: extremes in Southeastern Australia during the 1971–2022 period. Climate 12:75. https://doi.org/10.3390/cli12050075

Speer M, Leslie L (2024) Machine learning suggests climate and seasonal definitions should change under global warming. *Academia Environmental Sciences and Sustainability.* 2024–11–21. https://doi.org/10.20935/AcadEnvSci74

Srinivasan R, Carey-Smith T, Wang L, Harper A, Dean S, Macara G et al (2024) Moving to a new normal: analysis of shifting climate normals in New Zealand. Int J Climatol 44(10):1–24. https://doi.org/10.1002/joc.8521

Stips A, Macias D, Coughlan C, Garcia-Gorriz E, Liang XS (2016) On the causal structure between CO2 and global temperature. Sci Rep 6(1):21691. https://doi.org/10.1038/srep21691

Thomson DJ (1982) Spectrum estimation and harmonic analysis. Proc IEEE 70(9):1055–1096. https://doi.org/10.1109/PROC.1982.12433

Varotsos C, Assimakopoulos MN, Efstathiou M (2007) Technical note: long term memory effect in the atmospheric CO_2 concentration at Mana Loa. Atmos Chem Phys 7:629–634

Velasco E, Roth M (2010) Cities as net sources of CO_2: review of atmospheric CO_2 exchange in urban environments measured by eddy covariance. Geogr Compass 4(9):1238–1259

Verstraeten G, Poesen J, Demaree G, Salles C (2006) Long-term (105 years) variability in rain erosivity as derived from 10-min rainfall depth data for Ukkel (Brussels, Belgium): implications for assessing soil erosion rates. J Geophys Res 111:D22109

von Neumann J (1941) Distribution of the ratio of the mean square successive difference to the variance. Ann Math Stat 12:367–439

Von Storch H, Zwiers EW (2003) Statistical analysis in climate research. Cambridge University Press, Cambridge

White H (1980) A heteroskedasticity-consistent covariance matrix estimator and a direct test for heteroskedasticity. Econometrica 48(4):817–838. https://doi.org/10.2307/1912934

Winters PR (1960) Forecasting sales by exponentially weighted moving averages. Manag Sci 6(3):324–342

World Meteorological Organization/Global Atmosphere Watch (2003) GAW report – 227: WMO/GAW aerosol measurement procedures. Guidelines and Recommendations (WMO-No. 1177), Vol. 1177, 103

Wu DL et al (1995) A least-squares method for spectral analysis of space–time data. J Atmos Sci 52(20):3501–3510

Zhang X et al (2021) A small climate-amplifying effect of climate-carbon cycle interactions across timescales. Nat Commun 12:22392. https://doi.org/10.1038/s41467-021-22392-w

Zolina O, Simmer C, Gulev SG, Kollet S (2010) Changing structure of European precipitation: longer wet periods leading to more abundant rainfalls. Geophys Res Lett 37:L06704. https://doi.org/10.1029/2010GL042468